ON THE POSSIBILITY OF THE SOLAR FLARE ENERGY ACCUMULATION IN THE VICINITY OF A SINGULAR LINE

A. I. PODGORNY

P. N. Lebedev Physical Institute, USSR Academy of Sciences, 117924, Leninsky Prospect 53, Moscow, U.S.S.R.

(Received 11 December, 1988; in revised form 30 March, 1989)

Abstract. The energy of a solar flare can be accumulated as the magnetic energy of the current sheet created in the vicinity of a magnetic field singular line by the focusing of disturbances. Conditions which define the singular line in general were obtained using the properties of a singular line as it focuses disturbances. Numerical simulations and an analytical model show the possibility of the creation of a stable current sheet which becomes unstable after a quasistationary evolution. The nonlinear development of the instability leads to a fast reconstruction of the magnetic field with the release of a substantial part of the magnetic energy. The longitudinal magnetic field in our experiment increases the sheet thickness by at most a factoring of ten.

1. Introduction

The observations (see, for example, de Jager, 1985; Kahler *et al.*, 1986) give indications that the initial energy release in the solar flare takes place high in the solar corona. The problem is how the large quantity of energy ($\sim 10^{32}$ erg) accumulates in such a form as to be able to be released fast (during $\sim 10^3$ s). The magnetic energy can be accumulated in the vicinity of a magnetic field singular line (Syrovatsky, 1978a, b; Baum and Bratenahl, 1980) due to the self-focusing of MHD-disturbances with current sheet creation. This process was studied for the simple case of a singular line, namely the zero X-type magnetic line (in whose vicinity the magnetic field is $\overline{B} = \{-h_0 y, -h_0 x, 0\}$, where h_0 is the magnetic field gradient) and the hyperbolic field with a longitudinal component ($B = \{-h_0 y, -h_0 x, B_{z0}\}$). Using the properties of a singular line focusing MHD-disturbances in the above simple examples we try to find out the general conditions of singular line existence.

There is a point of view that the flare energy is stored slowly in a force-free field before it becomes unstable. Such fast energy release can be due to instabilities of current sheets which appear in the regions of reconnection of the force-free magnetic field. Therefore, this point of view does not contradict the possibility of a focusing process in the vicinity of a singular line.

There are many investigations which study different aspects of current sheet theory through different approaches. Some of the best known were proposed by Parker (1957), Sweet (1958), Harris (1962), Furth, Killen, and Rosenbluth (1963), Petschek (1964), Priest and Forbes (1986), Vasyliunas (1975), and Syrovatsky (1976). The review by Priest (1985) contains the latest results.

Here there is an attempt to answer an important question: Why during the magnetic energy accumulation does an instability not appear so that a quasi-stationary current

Solar Physics **123:** 285–308, 1989.

sheet can be created, but later an instability does appear and so leads to fast energy release?

The current sheet is created by plasma flow in the vicinity of the singular line and is reinforced by this flow throughout its existence. At first, the current sheet can be stable, but later the quasistationary evolution can lead it into an unstable state. Using the results of numerical calculation and some physical considerations which arise, particularly, from the models of Parker (1957) and Syrovatsky (1976), we propose a model for a quasi-stationary current sheet in which the total plasma mass in the sheet can slowly change with the course of time. Conditions are obtained for the quasi-stationary evolution of the current sheet which leads to the instability.

2. Singular Lines

The reconnection takes place if the magnetic field near the singular line has an X-type topology and $\partial B/\partial t$ electric field along this line can not be compensated (Syrovatsky, 1978a, b, Baum and Bratenahl, 1980; Greene, 1988; Hesse and Schindler, 1988; Schindler, Hesse, and Birn, 1988; Priest and Forbes, 1989). Also, for singular lines considered here, the disturbances appeared far from singular line must be focused to it causing the reconnection process. To deduce relationships which determine singular lines, considerations based on analogy with the disturbance focusing in a more simple case of a singular line in a hyperbolic field $\{B_x = -h_0 y,\ B_y = -h_0 x,\ B_{z0}\}$ are used.

It is possible that currents in the solar corona could not change the magnetic field topology so strongly as to vanish the singular lines of the potential field. New singular lines can appear in the force-free magnetic field, for example, between twisted magnetic tubes. The properties of singular lines are considered here for the potential magnetic field which can be found in the solar corona (see, for example, Den, Kornitska, and Molodensky, 1983) from observed magnetic field in the photosphere. These properties of singular lines can be generalized in the case of the force-free magnetic field which can be found in the solar corona under some conditions (see, for example, Gary *et al.*, 1987; Yang, Hong, and Ding, 1988).

Due to the high plasma conductivity, the magnetic field can be considered to be frozen into the plasma. The space in the vicinity of the line where the magnetic field is $\overline{B} = \{-h_0 y,\ -h_0 x,\ 0\}$ or $\overline{B} = \{-h_0 y,\ -h_0 x,\ B_{z0}\}$ is separated by the planes $(y = -x)$ and $(y = x)$ into four sectors with different magnetic fluxes so that MHD-disturbances are focused as follows. If the plasma flow is directed towards the line $\{x = 0,\ y = 0\}$ in two opposite sectors (for example, where the y-axis is placed) and plasma flows away from this line in two other opposite sectors, then the plasma flow distorts the magnetic field. The field is expanded in the x-direction and compressed in the y-direction. The current density increases, therefore the magnetic force $c^{-1}\bar{j} \times \overline{B}$ increases, too. This force propels plasma in the direction of the plasma flow. The plasma velocity grows and the plasma flow increases the deformation of the magnetic field creating a configuration with a current sheet. The magnetic energy accumulation stops when the current sheet thickness gets so small that the frozen-in condition is violated and all the magnetic

energy coming with the plasma flow into the sheet dissipates there:

$$a = \frac{\nu_m}{V_{\text{in}}}, \tag{1}$$

where V_{in} is the plasma inflow velocity to the sheet, 'a' is the sheet thickness, $\nu_m = c^2/4\pi\sigma$ is the magnetic diffusivity for the conductivity σ. Physically, it means that the electric field near the sheet ($E_{ns} = c^{-1} V_{\text{in}} B_s$, B_s is the value of the magnetic field near the sheet) is equal to that in the sheet ($E_s = j/\sigma = B_s/4\pi a\sigma$) (Parker, 1957).

Assuming that the process of MHD-disturbance focusing in the vicinity of a general-type singular line is similar to that described above, we can formulate the properties of the singular line as follows:

(1) The space in the vicinity of the singular line can be subdivided into four sectors by surfaces which intersect along the singular line so that every magnetic line is located entirely in one sector.

(2) If the electric current flows along the singular line, then the forces $c^{-1}\bar{j} \times \bar{B}$ in two opposite sectors are directed towards the singular line and in two other sectors away from it.

(3) If the frozen-in condition is fulfilled and plasma flows come into the vicinity of the singular line from two opposite sectors, then plasma flows from the other two sectors cannot carry out the magnetic field incoming with plasma in the first two sectors.

(4) On the singular line, there is no magnetic field component perpendicular to the singular line, so the induced electric field along the singular line created by the variation of the magnetic flux cannot be compensated by the field $c^{-1}\bar{V} \times \bar{B}$.

If the magnetic field differs from the field where conditions (1)–(4) are fulfilled, then only part of the magnetic energy is accumulated by the focusing process. Its other part goes out with plasma under the influence of the force $c^{-1}\bar{j} \times \bar{B}$ which is not equal to zero on the line, if condition 4 is not fulfilled. If the field does not strongly differ from that where conditions (1)–(4) are fulfilled, then the energy accumulation can be more effective than the energy exit and the solar flare energy can be stored.

At first, we find relationships on the singular line corresponding to ideal fulfillment of conditions (1)–(4) in potential field.

In the plane case (where B does not depend on z and $B_z(x, y) \equiv 0$) the singular line can be the only zero line (according to conditions (1)–(4)) and the zero line must be the only singular line, since in the linear expansion in its vicinity

$$B_x = a_{xx}x + a_{xy}y, \qquad B_y = a_{yx}x + a_{yy}y, \tag{2}$$

with $a_{xx} = -a_{yy}$ (since $\operatorname{div}\bar{B} = 0$) and $a_{yx} = a_{xy}$ (since $\operatorname{rot}\bar{B} = 0$). Turning the coordinate axes through the angle $\alpha = -\frac{1}{2}\operatorname{arctg}(a_{xy}/a_{xx})$ gives the well-known form $\bar{B} = \{-h_0 y, -h_0 x, 0\}$ where $h_0 = -a_{xy}/\cos(2\alpha)$.

To deduce the properties of a singular line in general we shall make clear why in a hyperbolic magnetic field with a longitudinal component

$$B_x = -h_0 y, \qquad B_y = -h_0 x, \qquad B_z = B_{z0}, \tag{3}$$

there are no points outside the Z-axis, through which the 'ideal' singular line can pass. For example, let us consider the point $(0, y_0, 0)$. The expansion of the magnetic field in the vicinity of this point is

$$B_{x1} = \left(\frac{-h_0 B_{z0}}{\sqrt{h_0^2 y_0^2 + B_{z0}^2}}\right) y_1 ;$$

$$B_{y1} = \left(\frac{-h_0 B_{z0}}{\sqrt{h_0^2 y_0^2 + B_{z0}^2}}\right) x_1 + \left(\frac{h_0^2 y_0}{\sqrt{h_0^2 y_0^2 + B_{z0}^2}}\right) z_1 ; \tag{4}$$

$$B_{z1} = \sqrt{h_0^2 y_0^2 + B_{z0}^2} + \left(\frac{h_0^2 y_0}{\sqrt{h_0^2 y_0^2 + B_{z0}^2}}\right) y_1 .$$

The z-axis is directed along the field; new coordinates are expressed in terms of the old ones by

$$x_1 = \frac{x B_{z0}}{\sqrt{h_0^2 y_0^2 + B_{z0}^2}} + \frac{z h_0 y_0}{\sqrt{h_0^2 y_0^2 + B_{z0}^2}} ; \qquad y_1 = y - y_0 ;$$

$$z_1 = \frac{-x h_0 y_0}{\sqrt{h_0^2 y_0^2 + B_{z0}^2}} + \frac{z B_{z0}}{\sqrt{h_0^2 y_0^2 + B_{z0}^2}} .$$

If $z_1 = 0$, then the expressions for B_{x1} and B_{y1} have the same form as in (3). But if $z_1 \neq 0$, the above type of field variation would be in the vicinity of the point $(x_1 = (h_0 y_0 / B_{z0}) z_1, y_1 = 0)$ rather than in the vicinity of the point $(x_1 = 0, y_1 = 0)$. Therefore, surfaces which divide the space into four sectors must intersect along the line $(x_1 = (h_0 y_0 / B_{z0}) z_1, y_1 = 0)$, where the magnetic field has a non-zero perpendicular component, because it is tangential to the line $(x_1 = 0, y_1 = 0)$. So, the line $(x_1 = (h_0 y_0 / B_{z0}) z_1, y_1 = 0)$ does not satisfy the property 4, and the singular line cannot pass through the point $(x = 0, y = y_0, z = 0)$.

A similar consideration for every point which does not lie on the z-axis gives an expansion of the type (4) which has a linear dependence of B_{x1} and (or) B_{y1} on z_1. Points of the singular line satisfy the condition

$$\frac{\partial B_{x1}}{\partial z_1} = 0 , \qquad \frac{\partial B_{y1}}{\partial z_1} = 0 \tag{5}$$

which we shall later consider to be necessary for the existence of a singular line. If on the singular line $\overline{B} \neq 0$, then the derivative $\partial / \partial z_1$ must be proportional to the derivative along the local field direction $(\overline{B}, \nabla)$, since z_1-axis is directed along $\overline{B}$. Condition (5) means that x_1- and y_1-components of $(\overline{B}, \nabla)\overline{B}$ are zero. It means that vector $(\overline{B}, \nabla)\overline{B}$ must be parallel to the z_1-axis and, therefore, to the vector $\overline{B}$. So, condition (5) means that the vector $(\overline{B}, \nabla)\overline{B}$ must be parallel to the vector $\overline{B}$ or

$$(\overline{B}, \nabla)\overline{B} \times \overline{B} = 0 . \tag{6}$$

Equation (6) describes a line in three-dimensional space, since out of the three scalar equations only two are independent. According to property 4, on the singular line there should not be any magnetic field component perpendicular to the singular line, so it is necessary to choose among all the lines satisfying condition (6) only those that coincide with magnetic field lines or zero-magnetic field lines.

To study the field in the vicinity of the line satisfying Equation (6) we should expand the field in this vicinity in the system of coordinates with the z-axis directed along the magnetic field:

$$\begin{aligned} B_x &= h_{xx}x + h_{xy}y + h_{xz}z\,, \\ B_y &= h_{yx}x + h_{yy}y + h_{yz}z\,, \\ B_z &= h_{zx}x + h_{zy}y + h_{zz}z + B_{z0}\,. \end{aligned} \tag{7}$$

It is clear that the potentiality of the field ($\operatorname{rot}\overline{B} = 0$) means the symmetry of the matrix

$$h_M = \begin{pmatrix} h_{xx} & h_{xy} & h_{xz} \\ h_{yx} & h_{yy} & h_{yz} \\ h_{zx} & h_{zy} & h_{zz} \end{pmatrix}, \tag{8}$$

i.e., $h_{xy} = h_{yx}$, $h_{xz} = h_{zx}$, $h_{yz} = h_{zy}$. Here $\operatorname{div}\overline{B} = 0$ means that $h_{xx} + h_{yy} + h_{zz} = 0$. Condition (5), and consequently (6), means that $h_{xz} = h_{yz} = 0$. In other words, vector $\overline{B}$ on the singular line (in our coordinates $(0, 0, B_z)$) is the eigenvector of the matrix h_M. As $h_{xy} = h_{yx}$, the coordinate system can be rotated about the z-axis so that $h_{xy} = h_{yx} = 0$. Therefore, the expansion in the vicinity of the line (6) is as follows:

$$B_x = h_x x\,, \tag{9}$$

$$B_y = h_y y\,, \tag{10}$$

$$B_z = h_z z + B_{z0}\,, \tag{11}$$

where $h_x + h_y + h_z = 0$. If $h_z = 0$, then this field is the well-known hyperbolic magnetic field with $B_z \neq 0$ (the system of coordinates where the field has the form $\{-h_0 y, -h_0 x, B_{z0}\}$ is recovered by turning through an angle $\frac{1}{4}\pi$).

If $h_z \neq 0$, it is necessary to study two cases: (a) signs of h_x and h_y are the same; (b) signs of h_x and h_y are opposite. Projections of magnetic lines on the plane (z, y) are described by the formula

$$y = Cx^{\alpha}\,, \tag{12}$$

where $\alpha = h_y/h_x$. If h_x and h_y have the same signs ($\alpha > 0$), then projections of magnetic lines have a parabolic shape (see Figure 1(a)) and division of the space into four sectors according to properties 1–3 is not possible. For the same reason this line cannot be singular in the two degenerate cases $h_x = 0$ and $h_y = 0$, when projections of magnetic lines on the plane (x, y) are straight lines parallel to the y-axis or to the z-axis (formally, if $h_x = 0$, we cannot use expression (12)).

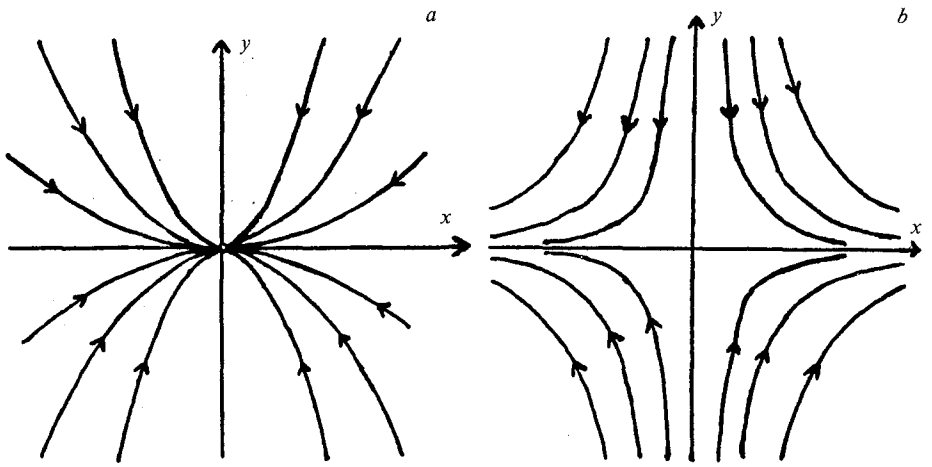

Fig. 1. The family of curves described by $y = cx^{\alpha}$; (a) $\alpha > 0$, (b) $\alpha < 0$.

In the case of h_x and h_y having opposite signs ($\alpha < 0$) projections of magnetic lines on the plane (x, y) are hyperbolas (Figure 1(b)). Planes (x, z) and (y, z) divide the space into four sectors according to property 1 and it is clear that all properties 1 to 4 are satisfied. So, if the signs of h_x and h_y are opposite and both of them are non-zero, then the line satisfying the condition (6) is singular and in the opposite case this line is not singular.

A similar investigation can be carried out for the vicinity of the point where the field becomes zero; choosing the coordinate system with the basic vectors being eigenvectors of the matrix h_M (8) we obtain an expansion like (9)–(11) with $B_{z0} = 0$. So, the lines where the condition (6) is satisfied or the magnetic field becomes zero are singular, if eigenvalues of the matrix h_M (8) corresponding to eigenvectors in the plane normal to singular line have opposite signs. These conditions can be generalized on the case of a force-free field. Indeed, condition $\bar{B} \times \mathrm{rot}\,\bar{B} = 0$ in the system of coordinates with the z-axis directed along the magnetic field means that $\partial B_x/\partial z = \partial B_z/\partial x$; $\partial B_y/\partial z = \partial B_z/\partial y$. Then in the expansion (7) $h_{xz} = h_{zx}$, $h_{yz} = h_{zy}$, but h_{xy} would not be equal to h_{yx} as it was for the potential field. It means that if eigenvalues of the matrix h_M (8) have opposite signs, then projections of magnetic lines on the plane (x, y) have X-type topology. These lines are described by (12) with $\alpha < 0$, but in the nonorthogonal system of coordinates. So, all conditions (1)–(4) are fulfilled.

Now we consider the singular line in the vicinity of which besides the energy accumulation due to disturbances focusing there is some energy exit with the plasma propelled by a small force $c^{-1}\bar{j} \times \bar{B}$. The force $\bar{j} \times \bar{B}$ exists on the line because $\bar{j}$ is not precisely parallel to $\bar{B}$. On this line relation (6) can be fulfilled only approximately. The accuracy of the fulfillment of (6) can be estimated under the following assumption. If the 'ideal' singular line exists (where condition (6) is fulfilled precisely), then the distance from the singular line to the 'ideal' singular line must be less than the region size. Instead

of (9)–(11) the expansion in the vicinity of this line is as follows:

$$B_x = h_x x + \alpha_x z\,, \tag{13}$$

$$B_y = h_y y + \alpha_y z\,, \tag{14}$$

$$B_z = h_z z + \alpha_x x + \alpha_y y + B_{z0}\,. \tag{15}$$

The distance from the point $\{0, 0, 0\}$ to the line where condition (6) is fulfilled in the field (13)–(15) (this line exists only in the field (13)–(15), but for the real field the nonlinear terms of expansion should be taken into account and the line where condition (6) is strictly fulfilled may not exist) less than $|\alpha B_{z0}/(\alpha^2 + h^2)|$ where $|h| = \max(|h_x|, |h_y|)$, $|\alpha| = \max(|\alpha_x|, |\alpha_y|$. The region size can be estimated as $|B_0/h|$ where B_0 is the average magnetic field in the active region. So, the condition for a singular line has a form:

$$\left|\frac{\alpha B_{z0}}{\alpha^2 + h^2}\right| \Big/ \left|\frac{B_0}{h}\right| \ll 1\,. \tag{16}$$

This condition can be used practically instead of condition (6) together with the condition $\mathrm{sign}(h_x) \neq \mathrm{sign}(h_y)$ for seeking singular lines in the coronal magnetic field.

Condition (16) chooses among all potential singular lines defined by Priest and Forbes (1989) ones in the vicinity of which the process of reconnection can be caused by small disturbance appearing far from the singular line. This disturbance leads to a focusing process and therefore, to electric field or plasma flow corresponding to reconnection.

3. Numerical Simulation of Current Sheet Creation and Its Quasi-Stationary Existence

The process of the current sheet creation and its further development was studied by numerically solving the two-dimensional system of MHD-equations in the region containing the X-type singular line (the magnetic field is $\overline{B} = \{-h_0 y, -h_0 x, 0\}$ (Podgorny and Syrovatsky, 1981a) or $\overline{B} = \{-h_0 y, -h_0 x, B_{z0}\}$ (Podgorny, 1983a). Processes for the X-type neutral line, but under different conditions, were studied by Stevenson (1972), Brushlinsky, Zaborov, and Syrovatsky (1980), and Biskamp (1986). The size of this region 'l', which is approximately equal to the size of the active region in the solar corona, was taken as the dimensionless unit of length. The thickness of a current sheet in the solar corona is so small that the memory size of modern computers is not sufficient for an MHD-simulation. So, the current sheet properties were studied for plasma parameters corresponding to a sheet thickness which is much larger than that in the solar corona, but still much smaller than the active region size. The principle of limited simulation was used (see, for example, Podgorny, 1978).

The linear solution for a MHD-wave (Syrovatsky, 1968) corresponding to an electric field directed along the singular line was used for the boundary conditions. This wave can be caused by disturbances coming from under the photosphere; the solution is valid

a long distance from the singular line. Due to the symmetry of initial and boundary conditions relative to the X- and Y-axes, the MHD equations were solved numerically in the quarter plane ($0 \le x \le 1$, $0 \le y \le 1$). We shall describe here the task for the general case $\bar{B} = \{-h_0 y, -h_0 x, B_{z0}\}$, where the longitudinal magnetic field B_{z0} may be either zero or non-zero.

As units for temperature, plasma density, and plasma pressure were taken their values at the initial moment of time T_r, ρ_r, and $p_r = T_r \rho_r$. As a unit of magnetic field the value of the transverse magnetic field at the boundary B_0 was taken. As the units of velocity, time and current density $V_0 = V_A = B_0/\sqrt{4\pi\rho_r}$, $t_0 = l/V_0$, and $j_0 = (c/4\pi)(B/l)$ were taken. The dimensionless system of MHD equations has the form:

$$\frac{\partial \bar{B}}{\partial t} = \operatorname{rot}(\bar{V} \times \bar{B}) - \frac{1}{R_m} \operatorname{rot}\left(\frac{\sigma_0}{\sigma} \operatorname{rot} \bar{B}\right), \tag{17}$$

$$\frac{\partial \rho}{\partial t} = -\operatorname{div}(\rho \bar{V}), \tag{18}$$

$$\frac{\partial \bar{V}}{\partial t} = -(\bar{V}, \nabla)\bar{V} - \frac{r_s^2}{\rho} \nabla(\rho T) - \frac{1}{\rho}(\bar{B} \times \operatorname{rot} \bar{B}) + \frac{1}{R\rho} \Delta \bar{V}, \tag{19}$$

$$\frac{\partial T}{\partial t} = -(\bar{V}, \nabla)T - (\gamma - 1)T \operatorname{div} \bar{V} + (\gamma - 1) \frac{\sigma_0}{R_m \sigma r_s^2 \rho} (\operatorname{rot} \bar{B})^2 - $$

$$- (\gamma - 1)GL'(T)\rho + \frac{\gamma - 1}{\pi\rho} \operatorname{div}\left(\frac{\kappa}{\kappa_0} \nabla T\right), \tag{20}$$

where $R_m = lV_0/\nu_m$ is the magnetic Reynolds number; $\nu_m = c^2/4\pi\sigma_0$; $\sigma/\sigma_0 = T^{-3/2}$; $r_s^2 = \beta/2 = 4\pi\rho_r T_r/B_0^2$; $\pi = \rho_r l V_0/\kappa_0$; $\kappa/\kappa_0 = T^{5/2}$; $R = \rho_0 l V_0/\eta$; κ, η, and $\gamma = \frac{5}{3}$ are thermal conductivity, viscosity, and the adiabatic constant; the term $(\gamma - 1)GL'(T)\rho$ describes the radiation cooling.

The initial conditions correspond to a motionless homogeneous plasma in the hyperbolic magnetic field:

$$\begin{aligned} &B_x = -y; \quad B_y = -x; \quad B_z = \frac{B_{z0}}{B_0}; \quad \rho = 1; \\ &V_x = 0; \quad V_y = 0; \quad V_z = 0; \quad T = 1. \end{aligned} \tag{21}$$

At the left and lower boundaries the following symmetry conditions were imposed for $x = 0$:

$$\begin{aligned} &\frac{\partial B_x}{\partial x} = 0; \quad B_y = 0; \quad \frac{\partial B_z}{\partial x} = 0; \quad \frac{\partial \rho}{\partial x} = 0; \\ &V_x = 0; \quad \frac{\partial V_z}{\partial x} = 0; \quad V_z = 0; \quad \frac{\partial T}{\partial x} = 0; \end{aligned} \tag{22}$$

for $y = 0$:

$$B_x = 0\,; \quad \frac{\partial B_y}{\partial y} = 0\,; \quad \frac{\partial B_z}{\partial y} = 0\,; \quad \frac{\partial \rho}{\partial y} = 0\,; \quad \frac{\partial V_x}{\partial y} = 0\,;$$
$$V_y = 0\,; \quad V_z = 0\,; \quad \frac{\partial T}{\partial y} = 0\,. \tag{23}$$

For the upper boundary of the region ($0 \leq x \leq 1$, $y = 1$) and for $0 \leq t \leq 1$ at the right boundary ($x = 1$, $0 \leq y \leq 1$) the following conditions were set:

$$B_x = -y - \frac{\varepsilon y}{x^2 + y^2}\,, \quad B_y = -x + \frac{\varepsilon x}{x^2 + y^2}\,, \quad B_z = \frac{B_{z0}}{B_0}\,,$$
$$\rho = 1\,, \quad V_x = \frac{\varepsilon x}{x^2 + y^2}\,, \quad V_y = \frac{-\varepsilon y}{x^2 + y^2}\,, \quad V_z = = 0\,, \quad T = 1\,, \tag{24}$$

where $\varepsilon = V_d/V_A \simeq \Delta B/B$ is the disturbance parameter, V_d is the inflow velocity at the boundary of the region. For $t > 1$ at the right boundary where the plasma flows out of the region, the conditions of free exit for ρ and $\overline{V}$ were given.

If we initially have $B_{z0} = 0$, $V_{z0} = 0$ and at the boundary $B_z = 0$, $V_z = 0$, then at every moment of time $B_z \equiv 0$, $V_z \equiv 0$ and we do not need to solve the equations for B_z and V_z.

In the case of $B_z = 0$ the three main parameters determining the sheet thickness and current density in the sheet are R_m, r_s^2, and ε. The most convenient parameters characterizing the current sheet are Syrovatsky numbers:

$$L = \varepsilon R_m \quad \text{and} \quad S = \varepsilon / r_s^2$$

which can be used instead of R_m and r_s^2. Parameters L and S actually are the ratios in order of magnitude between the terms which promote the creation of a thin current sheet and terms which counteract this process.

In order to compare the influences of the longitudinal magnetic field and the plasma pressure it is convenient to introduce the parameter S' which differs from S in such a way that the gas dynamical pressure is replaced by the sum of the plasma pressure and the pressure of the longitudinal magnetic field ($S' = \varepsilon/r_s'^2$; $r_s'^2 = r_s^2 + B_{z0}^2/2B_0^2$).

Most of our calculations were done for $3 \leq L$; S, $S' \leq 30$; $\varepsilon = 0.1$. The calculations were done on a nonuniform grid which was changing in time. The y-steps were small near the sheet ($b_{y\,\min} \simeq 10^{-2}$–$10^{-4}$) and they became smaller when the sheet got thinner so that it was 8–12 steps across the sheet.

The front of the MHD-wave which comes to the singular line at first, has a circle shape. Later it takes the form of an ellipse, since the velocity of the part of the wave where plasma comes to the singular line (in the present system of references – along the y-axis) is larger than the velocity in the part where the plasma goes out of the singular line (along the x-axis). After a while (for parameters L, S, and ε in our calculations this

time is $\sim 2t_0$) the ellipse 'flattens out' into the current sheet. In general the duration of the current sheet creation must be larger than the Alfvén time $t_0 = l/V_A$ and smaller than the plasma convection time $t_1 = l/V_d$, which agrees with the energy accumulation time for a solar flare.

The current density distribution which corresponds to the wave approaching the neutral point and distributions of the current density, plasma density, the pattern of magnetic lines and the plasma velocity field corresponding to the current sheet are represented in Figures 2–6. A schematic picture of the current sheet vicinity is given in Figure 7.

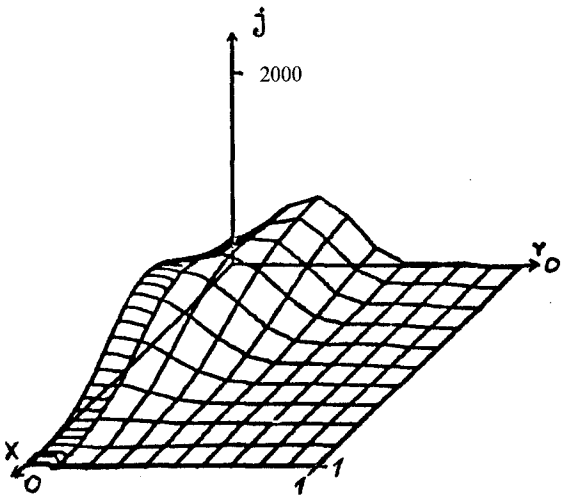

Fig. 2. The current density distribution in the quarter plane as a surface in three-dimensional space at the time $t = 1$ for $\varepsilon = 0.1$; $L = 3$, $S = 3$, $\pi = 100$.

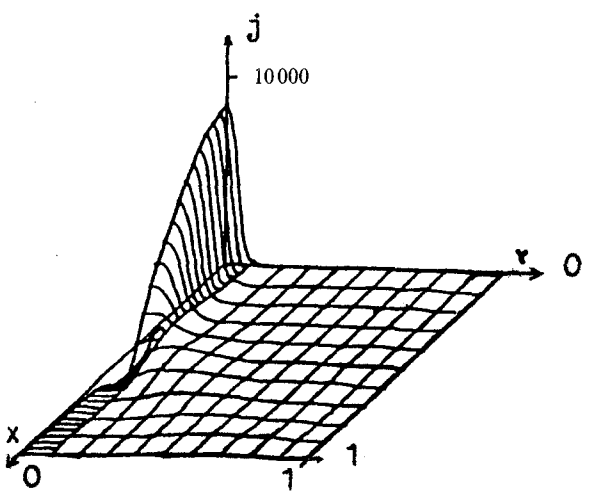

Fig. 3. The current density distribution at the time $t = 6$ for $\varepsilon = 0.1$; $L = 3$, $S = 3$, $\pi = 100$.

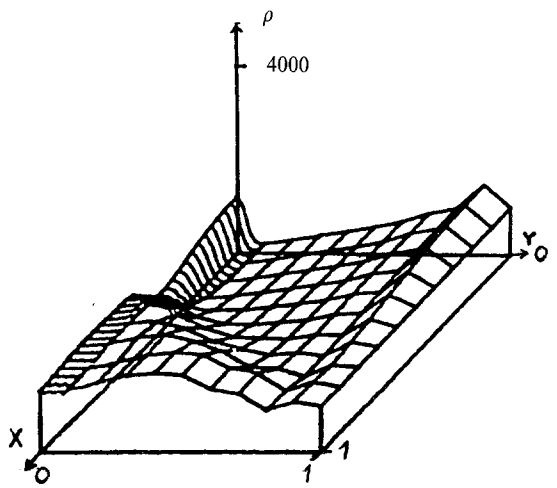

Fig. 4. The plasma density distribution at the time $t = 6$ for $\varepsilon = 0.1$; $L = 3$, $S = 3$, $\pi = 100$.

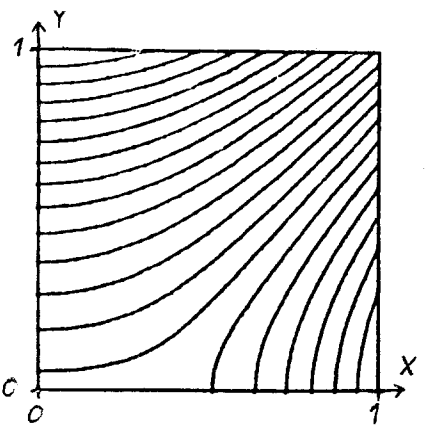

Fig. 5. The pattern of magnetic lines in the quarter plane at the time $t = 6$ for $\varepsilon = 0.1$; $L = 3$, $S = 3$, $\pi = 100$.

The plasma pressure increases in the sheet mainly because it counteracts the magnetic pressure and the plasma flow directed into the sheet. Being propelled chiefly by the magnetic tension force, the plasma goes along the sheet width and compresses the magnetic field directed normally to the sheet at the sheet edges. The plasma velocity at the sheet edges reaches a value of $0.4V_A$, which exceeds the local Alfvén velocity, so that fast shock waves appear at the sheet edges. Such an increase of the normal magnetic field corresponds to currents at the sheet edges which are directed oppositely to the current in the sheet.

In the quasi-stationary current sheet all the values slowly change with the course of time (the sheet becomes thinner, the current density increases), but among all of them the total plasma mass in the sheet undergoes the most rapid change – it decreases due to a fast plasma outflow.

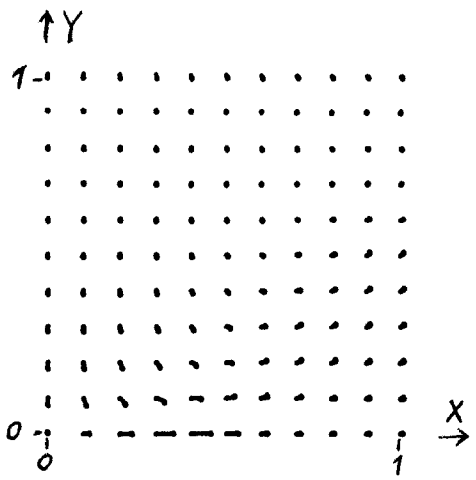

Fig. 6. The plasma velocities at the time $t = 6$ for $\varepsilon = 0.1$; $L = 3$, $S = 3$, $\pi = 100$.

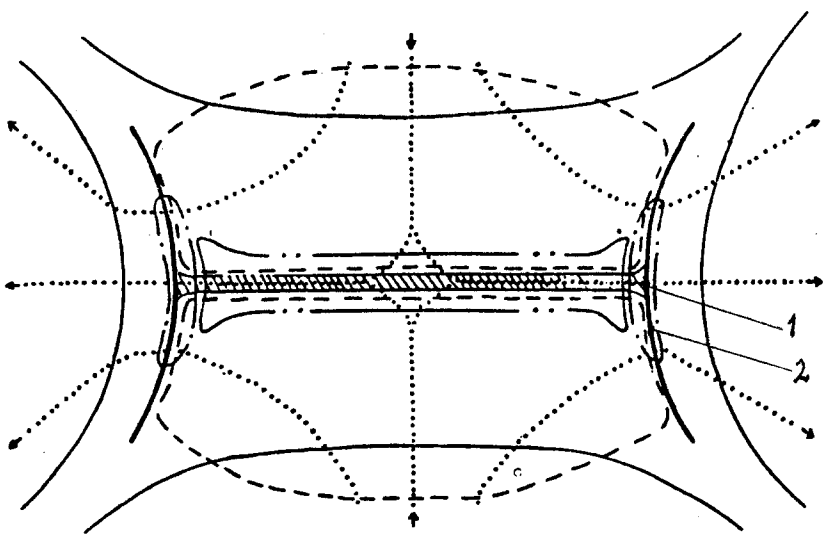

Fig. 7. The schematic picture of the behaviour in the vicinity of the current sheet. Magnetic lines are depicted by thin lines. Arrows show directions of plasma movement along the lines consisting of points. Fronts of shock waves are depicted by thick lines behind which the regions of the much increased plasma density and the compressed magnetic field are located. The region of increased plasma density is shaded. Regions bounded by lines are as follows: – · · – · · – region of increased current density; – · – · – · – regions of opposite current caused by compression of the magnetic field by the plasma flow leaving the sheet; – – – – – regions of low plasma density near the sheet. Points denoted by numbers indicate: 1 – variation of density at 1.5 times; 2 – variation of density at 4 times.

For symmetrical sets of L and S (i.e., $L = A$, $S = B$ and L = B, S = A) there is only a small difference in the behaviour of values in the sheet. In case of a slightly differing L and S, the ratio of the sheet width to its thickness is approximately equal to L or S (see Table I, and Podgorny, 1983a).

TABLE I

Half-thickness 'a', half-width 'b', their ratio 'b/a', current density 'j_z', plasma density 'ρ' and temperature 'T' in the centre of the sheet ($x = 0$, $y = 0$) expressed in dimensionless units at the time $t = 3$ and their dependence on L, S, S', and π

L	S	S'	π	a	b	b/a	j_z	ρ	T
30	30	–	10^2	0.009	0.43	48	56.6	10.11	4.70
30	30	–	10^5	0.0086	0.45	52	60.7	5.40	9.51
30	10	–	10^2	0.016	0.43	27	31.8	5.28	3.08
30	10	–	10^5	0.013	0.43	33	35.9	2.94	5.76
30	30	10	10^2	0.012	0.42	35	40.2	6.68	4.22
30	30	10	10^5	0.009	0.43	48	55.9	4.25	9.45
30	3	–	10^2	0.03	0.42	14	17.0	2.67	1.89
30	3	–	10^5	0.025	0.42	17	18.8	1.71	3.00
30	30	3	10^2	0.017	0.4	24	27.1	3.58	3.70
30	30	3	10^5	0.011	0.42	38	41.2	2.59	8.85
10	30	–	10^2	0.014	0.43	31	34.6	8.26	5.40
10	30	–	10^5	0.012	0.43	36	38.7	4.20	11.80
10	10	–	10^2	0.024	0.41	17	18.9	4.26	3.55
10	10	–	10^5	0.022	0.43	20	22.9	2.36	6.83
10	30	10	10^2	0.018	0.41	28	27.4	6.18	5.01
10	30	10	10^5	0.012	0.42	35	36.7	3.63	11.72
3	30	–	10^2	0.025	0.41	16	18.8	6.56	6.11
3	30	–	10^5	0.022	0.43	20	22.0	3.16	14.53
3	3	–	10^2	0.076	0.4	5	5.48	1.76	2.44
3	3	–	10^5	0.058	0.4	7	7.46	1.18	4.06

4. The Fast Magnetic Field Reconstruction: Numerical Results

Numerical calculations showed that for $L = 30$, $S = 30$ after the long quasi-stationary evolution, a fast reconstruction of the magnetic field and plasma flow occurs in the current sheet with the release of a substantial part of the magnetic energy (Podgorny, 1983b). The process of fast reconstruction in the sheet goes as follows. A preferable plasma inflow in the vicinity of the point $x = 0.2$ (dimensionless units) leads to magnetic field deformation which corresponds to a normal magnetic field component increase. Consequently, the magnetic tension force increases, which propels plasma out of this vicinity. The outflow velocity sharply increases and reaches a value exceeding the Alfvén velocity V_0. The pressure balance is violated in the vicinity of the point $x = 0.2$; under the influence of the magnetic pressure the inflow velocity in this vicinity grows (it reaches a value $\sim 0.1 V_A$). In the vicinity of the point $x = 0.2$ the current density and the magnetic dissipation increase. Then the plasma density (and consequently, the plasma pressure) in the vicinity of the point $x = 0.2$ substantially increases due to the strong increase of the inflow velocity. The inflow velocity in this vicinity decreases to a value which is smaller than that in the quasi-stationary sheet, so the current density in this vicinity also decreases to a value which is smaller than that in the quasi-stationary sheet. After the fast magnetic field reconstruction, which takes place during the period of several Alfvén times (2–3 t_0), there appears a configuration of the magnetic field with

the current density distribution having a local minimum in the vicinity of the point $x = 0.3$. This magnetic field configuration can exist in a quasi-stationary manner for $\sim 10\, t_0$ after the reconstruction. The current density distributions before and after the fast reconstruction are represented in Figures 8 and 9.

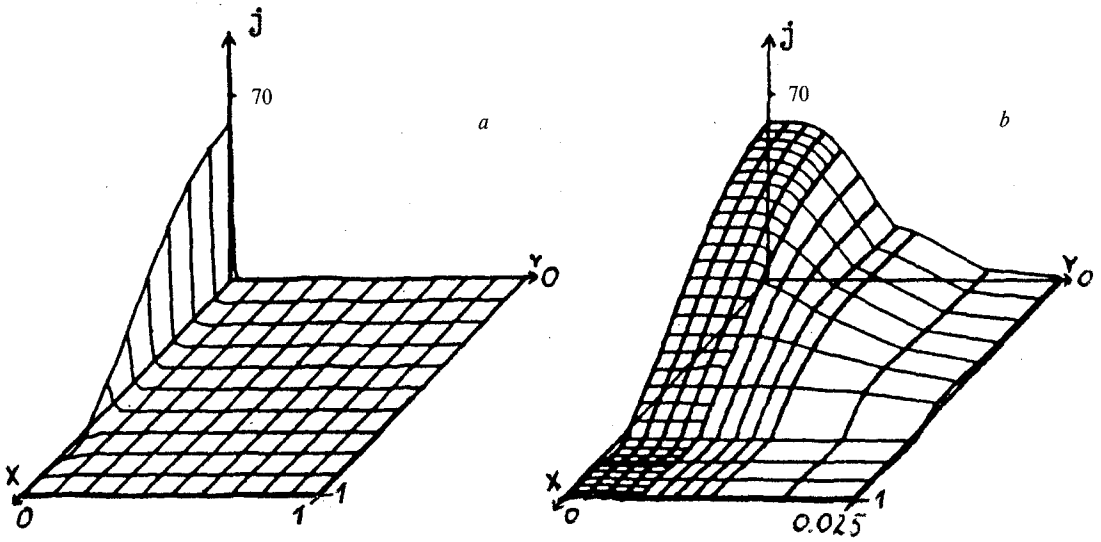

Fig. 8. The current density distribution at the time $t = 3$ for $\varepsilon = 0.1$; $L = 30$, $S = 30$, $\pi = 100$. (a) The scale on the y-axis is not stretched. (b) The scale on the y-axis is stretched 40 times.

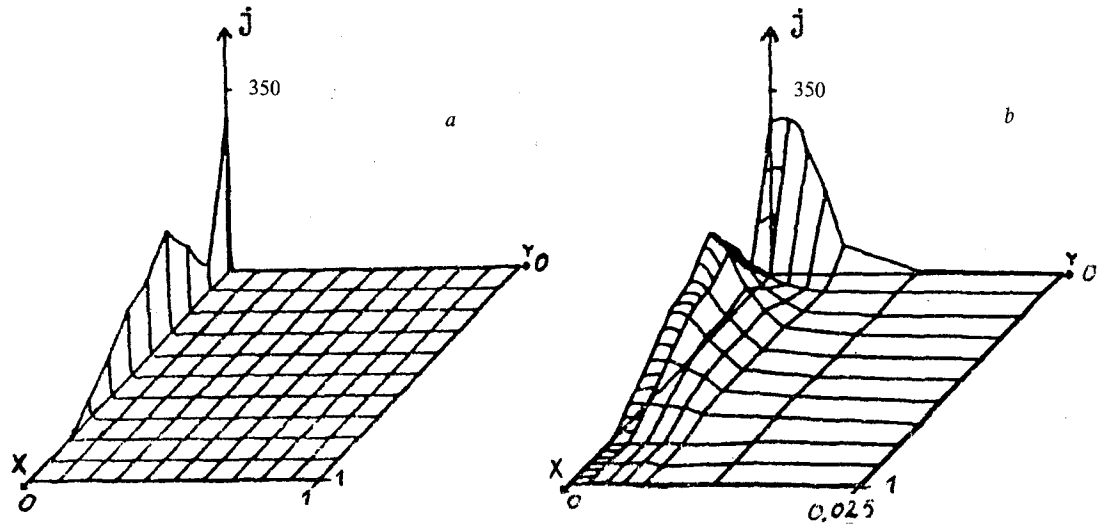

Fig. 9. The current density distribution at the time $t = 11$ for $\varepsilon = 0.1$; $L = 30$, $S = 30$, $\pi = 100$. (a) The scale on the y-axis is not stretched. (b) The scale on the y-axis is stretched 40 times.

5. Model of the Current Sheet

Our model of the current sheet represents a development of models proposed by Parker (1957) and Syrovatsky (1976) and contains an attempt to determine relations that describe the main interactions of values in the sheet. These relationships connect the values averaged across the sheet without taking into account the details of their distributions. The relationships represent the conservation laws obtained by the integration of the MHD equations. Taking Syrovatsky's (1976) model as a basis, Somov and Titov (1983) proposed a model of the turbulent current sheet with a more detailed account of thermal losses. For our model the information used was obtained by numerical MHD simulation of the current sheet created by disturbances in the vicinity of a singular line.

The basic distinguishing feature of this model is the lack of equality between plasma flows entering the sheet and leaving it (the total plasma mass of the sheet can slowly change in the course of time according to numerical simulation results). Other new elements are the propelling of the plasma along the sheet width mainly by the magnetic tension force (rather than by the plasma pressure) and the counteracting of the magnetic field pressure at the sheet edge by plasma flow from the sheet.

Unchangeability of the magnetic field with time ($\mathrm{rot}\,\overline{B} = 0$) in the two-dimensional case means that $E = \text{const}$. Equalizing the electric fields in the sheet and near the sheet we have the main equation (1) and equalizing the electric fields in the current sheet and at its edge ($c^{-1} V_{\text{out}} B_n$, where V_{out} is the plasma outflow velocity from the sheet, B_n is the magnetic field component normal to the sheet) we have

$$\frac{\nu_m B_s}{a} = V_{\text{out}} B_n \,. \tag{25}$$

This equation also has a magnetohydrodynamic interpretation: the diffusion of the normal magnetic field component into the sheet is equal to its exit with the plasma flow along the sheet width.

The plasma flow along the sheet width propelled mainly by the magnetic tension force $c^{-1} j B_y$ means

$$\rho_s V_x \frac{\mathrm{d}V_x}{\mathrm{d}x} = \frac{B_y(x) B_x}{4\pi a} \tag{26}$$

(ρ_s is the plasma density in the sheet). Taking into account a linear dependence of B_y on x ($B_y(x) = (B_n/b)x$, where b is the sheet width) which agrees with the numerical calculations, we can integrate (26) and obtain:

$$V_{\text{out}} = \sqrt{\frac{b}{a} \frac{B_n B_s}{4\pi\rho_s}} \,. \tag{27}$$

Taking into account a substantial deceleration of the plasma flow out of the sheet by the magnetic field pressure and approximating the value of the magnetic field at the sheet

edge with the initial hyperbolic field at this point ($h_0 b$) we have

$$\frac{\rho_s V_{\text{out}}^2}{2} = \frac{h_0^2 b^2}{8\pi} . \tag{28}$$

If ρ_s is known, then using (1), (25), (27), and (28) we can represent a, b, V_{out}, and B_n as functions of V_{in} and B_s:

$$a = \frac{v_m}{V_{\text{in}}} , \tag{29}$$

$$b = \frac{B_s^{3/2} V_{\text{in}}}{h_0^{3/2} V_{As}^{1/2} v_m^{1/2}} , \tag{30}$$

$$V_{\text{out}} = \frac{B_s^{1/2} V_{\text{in}} V_{As}^{1/2}}{h_0^{1/2} v_m^{1/2}} , \tag{31}$$

$$B_n = \frac{h_0^{1/2} v_m^{1/2} B_s^{1/2}}{V_{As}^{1/2}} , \tag{32}$$

where

$$V_{As} = \frac{B_s}{\sqrt{4\pi\rho_s}} .$$

To estimate the plasma density in the sheet we can use the balance of pressures in the sheet:

$$\rho_s T_s = \frac{B_s^2}{8\pi} \tag{33}$$

(T_s is the temperature in the sheet) and the balance of energy in the sheet. But it is difficult to estimate ρ_s in such a way, because we do not quite know all the mechanisms of the plasma cooling (thermal conductivity, radiation, outflow of hot plasma from the sheet), and so we are not sure we can accurately estimate thermal losses. The plasma density in the sheet must be maximal if the plasma cooling counteracts effectively the Joule heating so that the plasma temperature in the sheet does not increase compared with the temperature of the plasma in the active region of the corona. In this case the plasma density increases by $B_s^2/8\pi\rho_r \lesssim B_0^2/4\pi\rho_r \simeq \beta^{-1}$ times as compared with the plasma density of the coronal active region; estimates give $\rho_s/\rho_r \sim 10^6$. Observations show that in coronal arch-type structures the plasma density reaches $\sim 10^{11}$ cm^{-3}, which is three orders higher than in the corona ($\rho_r \sim 10^8$ cm^{-3}). It is impossible to observe structures with such a small size as the current sheet thickness where the plasma density can be larger than in the arch-type structures. So, it is natural to suppose that the range of the plasma density variation in the current sheet is $\rho_s/\rho_r \simeq 10^3$–$10^6$.

The velocity of the plasma flow into the sheet V_{in} decreases as compared to the inflow velocity into the region V_d due to the counterpressure of the 'magnetic pillow'. The latter

actually is the magnetic field which is accumulated near the sheet and could not dissipate in the sheet in time (Podgorny and Syrovatsky, 1981b). This situation corresponds to the pile-up solution in the classification of Priest and Forbes (1986). Using the numerical simulation results we can define that the maximum V_{in} is approximately equal to the inflow velocity at the region boundary (V_d) and the minimum V_{in} is several orders of magnitude lower than V_d, the maximum B_s is approximately equal to the magnetic field at the region boundary (B_0) and the minimum B_s is several times smaller than $0.1B_0$. These estimations agree with ones from the Priest–Forbes pile-up solutions.

Employing (29)–(32) we can obtain the criterion of the decrease of the total plasma mass in the sheet in the course of time:

$$\frac{V_{\text{in}} b \rho_r}{V_{\text{out}} a \rho_s} = \left(\frac{V_{\text{in}}}{V_{\text{A}}}\right)^2 R_m \sqrt{\frac{\rho_r}{\rho_s}} < 1 . \tag{34}$$

According to numerical calculations the total plasma mass in the sheet decreases in time in such a way that the plasma density in the middle of the sheet remains approximately unchanged and the plasma density near the sheet boundary (ρ_{ns}) decreases. This result can be physically interpreted through the analysis of the pressure balance in the sheet. The plasma density near the sheet boundary ρ_{ns} decreases in the course of time during the quasi-stationary evolution which takes place before the fast reconstruction according to the numerical simulation. Later we shall try to explain this fact by a study of the linear instability. So, condition (34) is a criterion for flare occurrence.

The small disturbances which are observed in the photosphere can produce MHD-waves of small amplitude. The magnetic field near the current sheet (B_s) created from such a small-amplitude wave can also be small. By this means it is possible to explain only small flares. The application of this model to large flares is more difficult because we must explain how the large magnetic field near the sheet (B_s) appears due to small-amplitude disturbance near the photosphere. Such a situation can take place because the mean value of the magnetic field in an active region near the photosphere is large. During the nonlinear propagation of this disturbance the field can be carried by a plasma flow to the singular line. But during the focusing process the magnetic field near the singular line is also dissipated due to the diffusion which is effective for small plasma conductivity. The plasma conductivity of the solar corona is high ($R_m = V_{\text{A}} l / v_m = 10^{16}$ or $V_d l / v_m = 10^8$–10^{10}), so it is possible to expect a large B_s even for a small inflow velocity in the photosphere, V_{d} ($V_d / V_{\text{A}} = 10^{-8}$–$10^{-6}$). The computer memory size is not sufficiently large to make calculations with such a large magnetic Reynolds number.

Taking parameters close to those in the corona, $T_r \sim 10^6$ K, $\rho_r \sim 10^8$ cm^{-3}, $B_r \sim 300$ G, the active region size $l_a \sim 10^{10}$ cm, and the outflow velocity on the photosphere $V_d \sim 10^3$–10^4 cm s^{-1}, we obtain $\sigma = 10^{16}$, $v_m = c^2/4\pi\sigma = 0.5 \times 10^4$, $V_{\text{A}} = B_0/\sqrt{4\pi\rho_r} = 0.5 \times 10^{10}$ cm s^{-1}, $R_m = l_a V_{\text{A}} / v_m = 10^{16}$, $V_d / V_{\text{A}} = 10^{-6}$–$10^{-7}$. For these parameters the dimensions of the current sheet from the model defined by (29)–(32) are approximately the same as in the Syrovatsky (1976) model: 'l' – 'b' × 'a' = $10^{10} \times 10^9 \times 10$ cm; for a magnetic field near the sheet of $B_s^2 \sim 300$ G

the magnetic energy of the sheet is about $B_s/8\pi b^2 l \simeq 10^{32}$ erg (the value of $b \sim 10^{10}$ cm corresponds better to the model (29)–(32) and for this value of b the value of B_s can be ~ 30 G to provide current sheet energy equal to $\sim 10^{32}$ erg, however, all relations (29)–(32) are obtained in order of magnitude, so we do not have any major differences in the current sheet dimensions from the Syrovatsky model). In the case when the inflow velocity does not decelerate under the influence of the magnetic field accumulated near the sheet ($V_{\text{in}}/V_d \simeq 1$), the criterion (34) is fulfilled for $\rho_r/\rho_s \simeq 10^{-3}$ if $V_d/V_{\text{A}} \lesssim 3 \times 10^{-8}$ and for $\rho_r/\rho_s \simeq 10^{-6}$ if $V_d/V_{\text{A}} \lesssim 3 \times 10^{-7}$. For $V_d/V_{\text{A}} \simeq 10^{-6}$ the criterion (34) is fulfilled even for the case of $\rho_r/\rho_s = 10^{-3}$ if the inflow velocity is decelerated by the magnetic field near the sheet so that $V_{\text{in}}/V_d \simeq 3 \times 10^{-2}$. So, there can be such a situation in the solar corona that criterion (34) for the current sheet is fulfilled and the fast energy release can occur. On the other hand, a current sheet which does not satisfy criterion (34) can exist in which the fast energy release does not occur, but rather the corona is slowly heated by magnetic field dissipation, as proposed by Browning, Sakurai, and Priest (1986).

6. Linear Analysis of MHD-Instability Associated with Magnetic Field Dissipation

Here we consider the linear disturbances V_{x1}, V_{y1}, B_{y1}, and ρ_1 for the sheet; initial values in the sheet are V_{x0}, V_{y0}, B_{y0}, ρ_0 ($V_{\text{in}0} = -V_{y0}(y = a)$, $V_{\text{in}1} = -V_{y1}(y = a)$). Instead of equation for B_x we use Equation (1) obtained from it – this is possible if the diffusion time for the sheet ($\tau_d = a^2/\nu_m = a/V_{\text{in}} = t_A/(V_{\text{in}}/V_{\text{A}})^2 R_m$) is much smaller than the instability development time γ^{-1} (this condition is fulfilled for the solar corona where $(V_{\text{in}}/V_{\text{A}})^2 R_m = 10^{-2}$–$10^{-4}$ and the instability duration is larger than $t_A = V_{\text{A}}^{-1}$, according both to the observations of the flare and to the value of the instability increment γ obtained below). Since the initial sheet thickness is $a_0 = \nu_m/V_{\text{in}0}$ and the perturbed sheet thickness is $a_1 = \nu_m/(V_{\text{in}0} + V_{\text{in}1})$, the disturbance of the current density is $j_1 = cB_s/4\pi a_1 - cB_s/4\pi a = cV_{\text{in}1}B_s/4\pi\nu_m$. The value of j is needed for us to know the disturbance of the magnetic tension force $c^{-1}jB_y$ which propels plasma along the sheet width and is a part of the equation for V_x.

The linear MHD-equations for disturbances are:

$$\rho_0 \frac{\partial V_{x1}}{\partial t} = -\rho_0 V_{x0} \frac{\partial V_{x1}}{\partial x} - \rho_0 V_{x1} \frac{\partial V_{x0}}{\partial x} - \rho_1 V_{x0} \frac{\partial V_{x0}}{\partial x} + \\ + \frac{1}{4\pi} B_{y0} \frac{B_x V_{\text{in}1}}{\nu_m} + \frac{1}{4\pi} B_{y1} \frac{B_x V_{\text{in}0}}{\nu_m} - \frac{\partial p_1}{\partial x}, \tag{35}$$

$$\rho_0 \frac{\partial V_{y1}}{\partial t} = -\rho_0 V_{x0} \frac{\partial V_{y1}}{\partial x} - \rho_0 V_{y1} \frac{\partial V_{y0}}{\partial y} - \rho_0 V_{y0} \frac{\partial V_{y1}}{\partial x} - \frac{\partial p_1}{\partial y} + \\ + \frac{1}{4\pi} B_x \frac{\partial B_{y1}}{\partial x}, \tag{36}$$

$$\frac{\partial \rho_1}{\partial t} = -V_{x0}\frac{\partial \rho_1}{\partial x} - \rho_1\frac{\partial V_{x0}}{\partial x} - \rho_0\frac{\partial V_{x1}}{\partial x} - \frac{\partial V_{y1}\rho_0}{\partial y}\,, \tag{37}$$

$$\frac{\partial B_{y1}}{\partial t} = -V_{x0}\frac{\partial B_{y1}}{\partial x} - V_{x1}\frac{\partial B_{y0}}{\partial x} - B_{y1}\frac{\partial V_{x0}}{\partial x} - B_{y0}\frac{\partial V_{x1}}{\partial x} + $$

$$+ B_x\frac{\partial V_{y1}}{\partial x} + \nu_m\frac{\partial^2 B_{y1}}{\partial x^2} + \nu_m\frac{\partial^2 B_{y1}}{\partial y^2}\,. \tag{38}$$

Values V_{x1}, V_{y1}, B_{y1}, and ρ_1 are represented in the form $e^{(\gamma t + ikx)}$, and we consider a perturbation with characteristic size equal to the sheet width $k^{-1} = b$, during which a substantial part of the release of current sheet magnetic energy should be expected. Using the fact of the existence of the characteristic size in the y-direction which is equal to the sheet thickness 'a' we have the equation for the instability increment γ:

$$\det\begin{pmatrix} -A-\gamma & \dfrac{B_s h}{4\pi\nu_m\rho_s} & \dfrac{1}{\rho_s}\left(\dfrac{T_s}{b^2} - A^2\right) & \dfrac{B_s}{4\pi a\rho_s} \\ 0 & k_V\dfrac{V_{\text{in}0}}{a} - \gamma & -k_p\dfrac{T_s}{a\rho_{ns}} & -\dfrac{B_s}{4\pi\rho_{ns}} \\ -\rho_s & \dfrac{\rho_{ns}}{a} & -A-\gamma & 0 \\ 2h & \dfrac{B_s}{b^2} & 0 & -A-\gamma \end{pmatrix} = 0\,, \tag{39}$$

(here $t_A^{-1} = V_A/l$ is taken as the unit for the dimensionless increment γ; $A = \partial V_{x0}/\partial x = V_{\text{out}}/b$, $h = \partial B_y/\partial x = B_n/b$ are taken from the model (29)–(32), $k_V, k_p < 1$ are the dimensionless coefficients for the transfer to finite differences $\rho_0\,\partial(V_{y1}V_{y0})/\partial y \simeq k_V\rho_{ns}V_{\text{in}0}V_{\text{in}}/a$, $\partial\rho_1 T_0/\partial y \simeq k_p T_s\rho_1/a$).

The physical meaning of this instability is as follows. The nonuniform plasma flow leads to an increase of the magnetic field normal to the sheet and consequently to an increase of the magnetic field tension force $c^{-1}jB_n$ which propels plasma out of the sheet. An additional increase of the magnetic tension force takes place due to the increase of the current density. The plasma outflow grows under the influence of the magnetic tension force and tends to decrease the plasma density and consequently the plasma pressure, and to increase the inflow velocity. A number of factors tend to stabilize the instability: the plasma inflow $\rho_{ns}V_{\text{in}}$ tries to increase the plasma density in the sheet, the plasma flow along the sheet with nonuniform velocity, the decrease of the magnetic field normal component due to magnetic diffusion, the decrease of the inflow velocity due to the magnetic tension force in the direction perpendicular to the sheet.

The plasma inflow $\rho_{ns} V_{in}$ depends on the plasma density near the sheet ρ_{ns}. So, our result concerning the instability appearance after the plasma density decrease near the sheet is physically clear.

The main differences between the instabilities considered here and those studied by Furth, Kilen, and Rosenbluth (1963), Dobrott, Prager, and Taylor (1977), and Bulanov, Sakai, and Syrovatsky (1979) are that here the plasma is compressible and the frozen-in condition in the sheet is violated due to the effective magnetic diffusion according to (1).

The analysis of Equation (39) shows that the mode with the maximum real part of the increment γ is aperiodic ($\operatorname{Im}\gamma = 0$) and for it:

$$\gamma_{\max} = \frac{1}{2} R_m^{-1} \left(\frac{V_{in0}}{V_A}\right)^{-2} + \sqrt{\left(\frac{1}{2} R_m^{-1} \left(\frac{V_{in0}}{V_A}\right)^{-2} \frac{\rho_r}{\rho_{ns}}\right)^2 + R_m^{-1} \left(\frac{V_{in0}}{V_A}\right)^{-2} \left(\frac{\rho_r}{\rho_s}\right)^{1/2} - 2\frac{\rho_r}{\rho_s}} + \sqrt{\frac{\rho_r}{\rho_s}} . \tag{40}$$

The condition of the instability $\gamma_{\max} > 0$ has the form

$$R_m \left(\frac{V_{in0}}{V_A}\right)^2 \sqrt{\frac{\rho_r}{\rho_s}} \frac{\rho_{ns}}{\rho_r} < \frac{1}{2} . \tag{41}$$

The situation in the solar corona can be such that immediately after the current sheet creation the condition of instability (41) is not fulfilled, but the condition of the plasma mass decrease (34) is fulfilled. Later the plasma density decrease at the sheet boundary during the quasi-stationary evolution condition (41) becomes fulfilled and the instability associated with the flare release of energy occurs.

During the development of the instability the plasma density near the sheet ρ_{ns} decreases, The instability increment (40) increases as ρ_{ns} decreases, so the instability grows strongly during the nonlinear phase. The magnetic field reconstruction in the sheet proceeds most effectively in a nonlinear phase if the inflow velocity in the sheet becomes approximately equal to the thermal velocity. In the balance of pressures obtained through integrating Equation (19) for the y-component of the momentum

$$p_s = \frac{B_s^2}{8\pi} + \int_0^a \rho \frac{\partial (V_y^2/2)}{\partial y} \, dy , \tag{42}$$

we can estimate $\int_0^a \rho(\partial V_y/2)/\partial y \, dy$ as $k\rho_s(V_{yM}/2)$, where V_{yM} is the maximum value of V_y for $0 \leq y \leq a$, $k \lesssim 1$. Taking into account that $p_s = \rho_s T_s$ we obtain

$$\rho_s = \frac{B_s^2/8}{T_s - kV_{yM}^2/2} . \tag{43}$$

If V_y becomes so large that $kV_{yM}^2/2 > T_s$, then expression (43) becomes meaningless. It means that the stationary state described by Equation (42) cannot be reached and the inflow velocity V_y must increase with time until the magnetic field dissipates, i.e., until the numerator in (43) becomes zero.

7. Influence of Longitudinal Magnetic Field

The longitudinal magnetic field is compressed in the sheet, and its pressure is directed against the plasma inflow velocity, so its influence is similar to the effect of plasma pressure. However, due to the effective magnetic diffusion in the sheet, the longitudinal magnetic field does not have an overwhelming effect on the parameters of the sheet (see Table I).

The distribution of the longitudinal magnetic field component and magnetic lines in three-dimensional space obtained by numerical simulations (the initial magnetic field was $B = \{-h_0 y, -h_0 x, B_{z0}\}$) are represented in Figures 10 and 11. Figure 12 shows

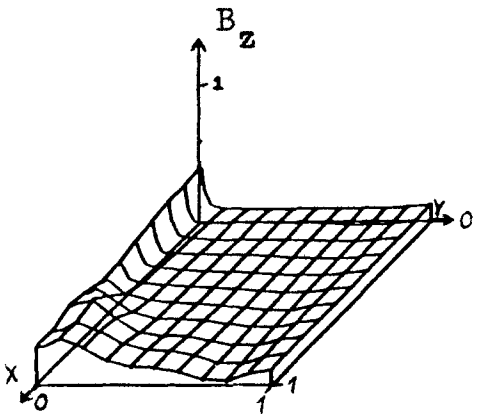

Fig. 10. Z-component magnetic field distribution for $\varepsilon = 0.1$; $L = 30$, $S = 30$, $S' = 10$, $\pi = 100$ at the time $t = 3$.

the dependence of the current density j_z, plasma density ρ, and the longitudinal magnetic field component B_z on the coordinate y perpendicular to the current sheet – it shows that B_z changes much more smoothly than j_z and ρ because of the magnetic diffusion.

We can estimate the increase of the longitudinal magnetic field in the sheet B_{zs} as compared with its value near the sheet B_{zns} using the equation

$$\mathrm{rot}(\overline{E} \cdot c) = 0\,, \tag{44}$$

where $\overline{E} \cdot c = -\overline{V} \times \overline{B} + \nu_m \,\mathrm{rot}\,\overline{B}$.

Equation (44) corresponds to the dimensionless equation for the quasi-stationary magnetic field ($\partial \overline{B}/\partial t \simeq 0$). In our case all the values do not depend on z. The x-component of Equation (44), $\partial(E_z c)/\partial y = 0$, implies that $E_z(y)c = \mathrm{const}$. Equalizing the value near the sheet, $E_z(y \simeq a)c = V_{\mathrm{in}} B_s$, to the value in the sheet,

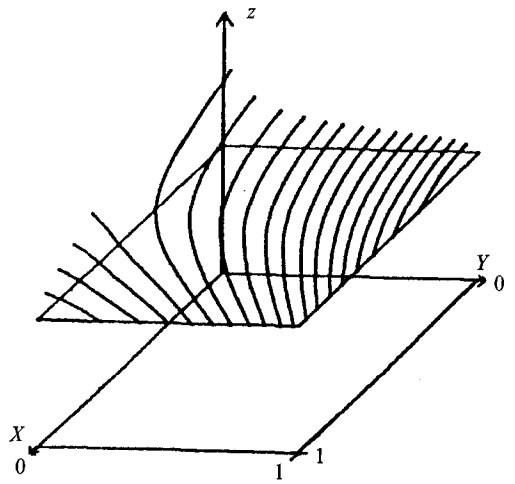

Fig. 11. Magnetic lines in three-dimensional space for $\varepsilon = 0, 1$; $L = 30$, $S = 30$, $S' = 10$, $\pi = 100$ at the time $t = 3$.

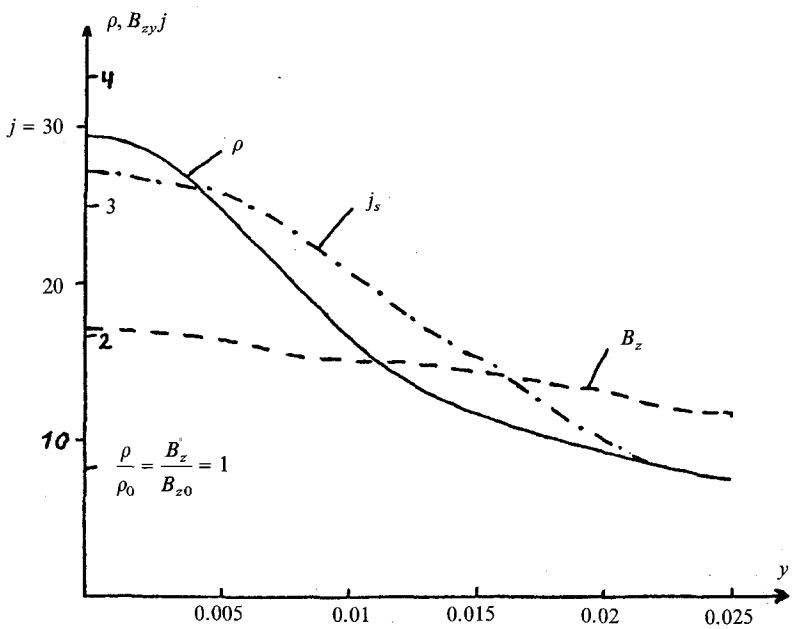

Fig. 12. Dependence of the plasma density ρ, z-component of the current density j_z and the longitudinal magnetic field B_z on the y-coordinate perpendicular to the sheet ($x = 0$) for $\varepsilon = 0, 1$; $L = 30$, $S = 30$, $S' = 3$, $\pi = 100$ at the time $t = 3$.

$E_z(y = 0)c = \nu_m(\partial B_z/\partial Y) = \nu_m(B_s/a)$, we obtain the well-known Equation (1). Using the z-component of Equation (44), $\partial(E_y c)/\partial x - \partial(E_x c)/\partial y = 0$, estimating $\partial(E_x c)/\partial y = a^{-1}(V_{\text{in}} B_{zns} - \nu_m(B_{zs} - B_{zns}/a))$ and $\partial(E_y c)/\partial x = V_{\text{out}} B_{ns}/b$, and employing (1) we have

(1) we have

$$B_{zs} = \frac{2B_{zns}}{1 + (aV_{\text{out}}/bV_{\text{in}})} = \frac{2B_{zns}}{1 + (V_{\text{in}}/V_{\text{A}})^{-2} R_m^{-1} \sqrt{\rho_{ns}/\rho_s}} . \tag{45}$$

The latter equality was obtained by using the model (29)–(32). The value of the longitudinal magnetic field in the sheet (45) corresponds to a balance between the increase of the longitudinal magnetic field in the sheet due to the inflow $V_{\text{in}}B_{zns}$ and a decrease of this value due to diffusion $v_m(B_{zs} - B_{zns}/a)$ and outflow $V_{\text{out}}B_{zs}$. To make an upper estimation we should neglect the exit of B together with the plasma flow out of the sheet ($V_{\text{out}} = 0$) and we obtain $B_{zs} \simeq 2B_{zns}$. The numerical simulation shows that $B_{zs} \simeq 1.3B_{zns}$ in the range of the plasma parameters' variation for which the computer memory size permits us to do calculations. Therefore, the pressure of the longitudinal magnetic field $B_s^2/8\pi$ must not increase in the sheet more than 4 times (according to the numerical simulation, in ~ 1.7 times) and at the same time the plasma pressure increases in the sheet by several orders of magnitude. Extrapolating the influence of the plasma pressure on the sheet parameters to the situation in the solar corona with a much larger Reynolds number obtained from the numerical simulation and using the estimate (45) we find that the addition of a longitudinal magnetic field of the same order as the transverse magnetic field is likely to increase the current sheet thickness by at most 10 times.

8. Conclusions

The instability analysis of the quasi-stationary current sheet shows the principal possibility of flare release of magnetic energy which was previously accumulated in the solar corona. More accurate analysis of the instability requires finding eigenvalues of the system of linear ordinary differential equations rather than of the system of linear algebraic equations. A further study must include also a study of the nonlinear phase of the instability by numerically solving the magnetohydrodynamic equations with the largest magnetic Reynolds number permitted by modern computers. The conditions under which the numerical simulation must be carried out are defined particularly by the condition of the linear instability obtained here.

Another direction for future investigations is the creation of a magnetic energy accumulation model for the solar flare in the coronal magnetic field of solar active region. This model must improve the solar flares' prognosis which up to now has been made purely phenomenologically without using any accurate physical theory. For this purpose we suggest that the present study permits us to understand a mechanism for the accumulation and fast release of magnetic energy in the current sheet. This model consists of the following:

(1) Finding singular lines in the coronal magnetic field using conditions (6) and (16) and analysing signs of eigenvalues of the matrix $\nabla \overline{B}$ (8). The magnetic field is approximated by a potential field which can be found using the observed magnetic field in the photosphere.

(2) The simulation of magnetic energy accumulation by focusing disturbances in the vicinity of the singular line with the creation of a current sheet. The initial magnetic field is potential and the boundary condition for disturbances is obtained from observations of the inflow velocity in the photosphere.

(3) Investigations of the possibility of fast energy release in the current sheet using analytical conditions (34), (41) and simulating numerically linear and especially nonlinear phases of the instability with a more detailed numerical set near the current sheet.

Acknowledgements

I wish to thank Professor I. M. Podgorny and the referee Professor E. Priest for useful comments and corrections.

References

Baum, P. J. and Bratenahl, A.: 1980, *Solar Phys.* **58**, 89.
Biskamp, S.: 1986, *Phys. Fluids* **29**, 1520.
Browning, P. K., Sakurai, T., and Priest, E. R.: 1986, *Astron. Astrophys.* **158**, 217.
Brushlinsky, K. V., Zaborov, A. M., and Syrovatsky, S. I.: 1980, *Fiz. Plasmy USSR* **6**, 297.
Bulanov, S. V., Sakai, J., and Syrovatsky, S. I.: 1979, *Fiz. Plasmy USSR* **5**, 280.
de Jager, C.: 1985, *Solar Phys.* **98**, 267.
Den, O. G., Kornitska, E. A., and Molodensky, M. M.: 1983, *Problems of Solar Flares*, Moscow, p. 72.
Dobrott, D., Prager, S. C., and Taylor, J.: 1977, *Phys. Fluids* **20**, 1850.
Furth, H. P., Killen, J., and Rosenbluth, M. N.: 1963, *Phys. Fluids* **6**, 459.
Gary, G. A., Moore, R. L., Hagyard, M. J., and Haisch, B. M.: 1987, *Astrophys. J.* **314**, 782.
Greene, J. M.: 1988, *J. Geophys. Res.* **93**, 8583.
Harris, E. G.: 1962, *Nuovo Cimento* **23**, 115.
Hesse, M. and Schindler, K.: 1988, *J. Geophys. Res.* **93**, 5559.
Kahler, S. W., Cliver, E. W., Cane, H. V., McCuire, R. E., Stone, R. G., and Sheely, N. R., Jr.: 1986, *Astrophys. J.* **302**, 504.
Parker, P. A.: 1957, *J. Geophys. Res.* **62**, 509.
Petschek, H. E.: 1964, *Proc. AAS–NASA Symposium of Physics of Solar Flares*, p. 425.
Podgorny, I. M.: 1978, *Fund. Cosmic Phys.* **1**, 1.
Podgorny, A. I.: 1983a, Preprint of Lebedev Inst. No. 84 (in Russian).
Podgorny, A. I.: 1983b, Preprint of Lebedev Inst. No. 17 (in Russian).
Podgorny, A. I. and Syrovatsky, S. I.: 1981a, *Fiz. Plasmy USSR* **7**, 1055.
Podgorny, A. I. and Syrovatsky, S. I.: 1981b, *Kosmich Issledovania USSR* **19**, 125.
Priest, E. R.: 1985, *Rep. Proc. Phys.* **48**, 955.
Priest, E. R. and Forbes, T. G.: 1986, *J. Geophys. Res.* **91**, 5579.
Priest, E. R. and Forbes, T. G.: 1989, *Solar Phys.* **119**, 211.
Schindler, K., Hesse, M., and Birn, J.: 1988, *J. Geophys. Res.* **93**, 5547.
Somov, B. V. and Titov, V. S.: 1983, *Astron. J. USSR Letters* **9**, 48.
Stevenson, J. C.: 1972, *J. Plasma Phys.* **7**, 293.
Sweet, P. A.: 1958, in B. Lehnert (ed.), *Electromagnetic Phenomena in Cosmic Physics*, Cambridge Univ. Press. Cambridge, p. 123.
Syrovatsky, S. I.: 1968, *Zh. Eksperim. Teor. Fiz. USSR* **54**, 1422.
Syrovatsky, S. I.: 1976, *Astron. J. USSR Letters* **2**, 35.
Syrovatsky, S. I.: 1978a, *Solar Phys.* **58**, 89.
Syrovatsky, S. I.: 1978b, *Astrophys. Space Sci.* **59**, 3.
Vasyliunas, M.: 1975, *Rev. Geophys. Space Phys.* **13**, 303.
Yang, H.-S., Hong, Q. F. and Ding, Y. J.: 1988, *Solar Phys.* **117**, 57.